DNA damage, nucleolar stress and dysregulated energy metabolism as mechanisms of multimorbidity.

Kristina Tomkova[1,6], Marius Roman[1,6], Adewale S Adebayo[1], Sophia Sheikh[1], Syabira Yusoff[1,3], Melanie Gulston[2], Lathishia Joel-David[1], Florence Y Lai[1], Antonio Murgia[2], Bryony Eagle-Hemming[1], Hardeep Aujla[1], Gavin D Richardson[5], Julian L Griffin[2,4], Gavin J Murphy[1], Marcin J Woźniak[1*]

Affiliations: [1] Department of Cardiovascular Sciences and NIHR Cardiovascular Biomedical Research Unit, University of Leicester, Glenfield Hospital, Leicester, LE3 9QP, UK;
[2] Department of Biochemistry and Cambridge Systems Biology Centre, The Sanger Building, 80 Tennis Court Road, Cambridge, CB2 1GA
[3] Cardiovascular Sciences, King's College London, London, UK
[4] Biomolecular Medicine, Department of Metabolism, Digestion and Reproduction, The Sir Alexander Fleming Building, Imperial College London, Exhibition Road, South Kensington, London, SW7 2AZ, UK.
[5] Biosciences Institute, Vascular Biology and Medicine Theme, Faculty of Medical Sciences, Newcastle University, Newcastle Upon Tyne, UK.
[6] Miss Tomkova and Dr Roman contributed equally.

* **Corresponding Author:** Dr Marcin J Woźniak Department of Cardiovascular Sciences, University of Leicester, Clinical Sciences Wing, Glenfield General Hospital, Leicester, LE3 9QP, UK. Tel: +44 116 258 3028, Email: mw299@leicester.ac.uk

Short title: Mechanisms of multimorbidity

Word count:

Keywords: Myocardium, Frailty, Multimorbidity, Cellular Senescence, DNA Damage, Cell Nucleolus, Energy Metabolism, Innate immunity

Abstract

Background Two-thirds of people over 65 have two or more underlying chronic conditions. Patients with multimorbidities are likely to classify as frail and have worse outcomes after cardiac surgery. We hypothesized that metabolite and transcript profiles could identify multimorbidity-specific mechanisms for clinical interventions.

Methods and Results The multimorbidity was defined as two or more coexisting chronic conditions. Analysis of the metabolome was performed in 30 sequential patients. Measurements of transcriptome and metabolites involved in energy production were performed in 53 and 57 sequential patients, respectively. Mitochondrial function in circulating monocytes was performed in 63 sequential patients. Our analysis distinguished three major processes that are affected by multimorbidity: innate immune response, DNA damage and associated epigenetic changes, and mitochondrial energy production. The innate immune response was upregulated in multimorbidity and most of the included comorbidities. The DNA damage, epigenetic changes and aspects of mitochondrial function were specific for multimorbidity. Histone 2B, its ubiquitination enzymes and AKT3 were upregulated in the multimorbid group suggesting senescence-like changes in gene expression. That was confirmed by the detection of senescence-associated secretory phenotype analytes, IL-1β, its receptor and fractalkine that increased with the number of accumulating comorbidities. DNA damage was confirmed by independent immunohistochemistry experiments, which also identified nucleolar instability as more prominent in the multimorbid myocardium. The nucleolar stress is potentially responsible for higher expression of ribosomal proteins and decreased mitochondrial function.

Conclusions Our results suggest that accumulating comorbidities increase levels of innate immune response and lead to DNA damage, senescence-like changes in gene expression and consequently decreased mitochondrial function.

Introduction

Multimorbidity is defined as the coexistence of two or more chronic conditions, with more than three-quarters of individuals with multimorbidities being classified as frail. [1] Patients with multimorbidity are more vulnerable to stressors, and even a minor health issue can severely affect their well-being and survival. [2] The incidence of multimorbidity and frailty is predicted to increase in the next two decades. [3] Both conditions are prevalent in ageing populations and in patients from socioeconomically deprived areas or with mental health diseases. [3,4] Multimorbidity is also present in more than two-thirds of the cardiovascular disease population. [5] These patients are more likely to die during cardiac surgery or develop complications. [6] Multimorbidity is multi-factorial, and metabolites and gene expression profiles likely depend on composite comorbidities. [7] Despite the significant effect of multimorbidity on post-surgery mortality, the underlying mechanisms are poorly understood. [8] As a result of this knowledge gap, exploring expression patterns of metabolites and genes in tissues can provide insights into the unifying mechanisms common to all patients with multimorbidities.

Previous evidence suggests that disruption of energy production and long-term oxidative stress caused by increased inflammation levels as potential mechanisms underlying multimorbidity. [9–11] In the present study, we report an analysis of transcriptomics in heart biopsies, metabolomics in heart biopsies and paired plasma samples and mitochondrial respiration analysis in circulating monocytes. We hypothesize that transcripts and metabolite expression patterns can point towards mechanisms specific to multimorbidity.

Methods

Study design ObCard was a prospective observational study approved by The East Midlands – Nottingham 1 Research Ethics Committee. All participants provided written informed consent. The study protocol was registered at https://clinicaltrials.gov/ct2/show/NCT02908009. The study is reported as per the STrengthening the Reporting of Observational studies in Epidemiology (STROBE) statement. [12] The STROBE checklist is included as **Table S1**. The study adhered to the principles outlined in the Declaration of Helsinki.

Study cohort Adult cardiac surgery patients (>16 years) undergoing coronary artery bypass grafting with or without valve surgery. Patients with pre-existing paroxysmal, persistent or chronic atrial fibrillation, pre-existing inflammatory state (sepsis undergoing treatment, acute kidney injury within five days, chronic inflammatory disease, congestive heart failure), ejection fraction <30 %, pregnancy and in a critical pre-operative state (Kidney Disease: Improving Global Outcomes (KDIGO) Stage 3 AKI [13] or requiring inotropes, ventilation or intra-aortic balloon pump) were excluded. Emergency or salvage procedure was also excluded. This was an exploratory study. The sample size was based on published case-control studies that have measured similar endpoints. [14,15] Missing data of 10-15% due to non-compliance or drop-out was accepted and included in the sample size calculation. Patients were classified as multimorbid if they had two or more comorbidities.

Sampling Right atrial biopsies were collected in a standardized manner from the right auriculum prior to placing the patients on cardiopulmonary bypass and were immediately snap-frozen in liquid nitrogen.

Outcomes: changes in transcripts and metabolites expression profiles in atrial biopsies; mitochondrial respiration in circulating monocytes.

Measures taken to reduce bias Detection bias was minimized by blinding laboratory staff analyzing right atrial biopsies and blood samples that will be identified only by a trial ID and the time of sample collection.

RNA isolation and sequencing RNA was isolated from 20mg of tissue using Isolate II RNA mini kit (Bioline, London, UK). Sample quality was assessed using the RNA Screentape assay on the Agilent TapeStation 4200. Only samples with RNA integrity numbers equal to or greater than eight were sequenced.

Library preparation and sequencing were carried out in two batches by Source BioScience (Nottingham, UK). The stranded total RNA libraries were prepared in accordance with the Illumina TruSeq stranded total RNA sample preparation guide with Ribo-Zero

human/mouse/rat for Illumina paired-end multiplexed sequencing. The libraries were validated on the Agilent Bioanalyzer 2100 to check the size distribution of the libraries and on the Qubit high sensitivity to check the concentration of the libraries. Sequencing was performed using 75bp paired-end chemistry on HiSeq 4000 with the TruSeq stranded total RNA human kit.

Metabolomics

Untargeted metabolomics was performed by Metabolon, Inc. (USA). All samples passed appropriate quality controls.

A panel of 144 cellular metabolites involved in mitochondrial function and energy metabolism were analyzed using a targeted assay on a Thermo Qunativa interfaced with a Vanquish LC as previously described in. [16,17] In brief, tissue was extracted using a modified Folch extraction into chloroform/methanol (2:1 600 ul per 50 mg of tissue, followed by 200 ul of water, 200 ul of chloroform, repeated once). For nucleotides and acyl-CoA derivatives, one-half of the aqueous extract was dissolved in 150 µl of 70:30 acetonitrile:water containing 20 µM deoxy-glucose 6 phosphate and 20 µM [U−13C, 15N] glutamate. The resulting solution was vortexed, sonicated and centrifuged. Chromatography consisted of a strong mobile phase (A) was 100 mM ammonium acetate, and the weak mobile phase was acetonitrile (B) and the LC column used was the ZIC-HILIC column from Sequant (100 mm × 2.1 mm, 5 µm).

For amino acids and TCA cycle intermediates, aqueous extracts were reconstituted in 50 µl of 10 mmol/l ammonium acetate in water before TCA cycle intermediates were separated using reversed-phase liquid chromatography on a C18-PFP column (150 mm × 2.1 mm, 2.0 µm; ACE). For chromatography on the UHPLC system, mobile phase A was 0.1% formic acid in water, and mobile phase B was 0.1% formic acid in acetonitrile. Mass transitions of each species were as follows (precursor > product): D5-L-proline 121.2 > 74.2; D8-L-valine 126.1 > 80.2; D10-L-leucine 142.0 > 96.2; L-glutamate [M] 148.0 > 84.2; L-glutamate [M+1] 149.0 > 85.2; L-glutamate [M+6] 154.1 > 89.1; citrate 191.0 > 111.0; citrate [M+1] 192.0 > 112.0; citrate [M+2] 193.0 > 113.0; citrate [M+3] 194.0 > 114.0; citrate [M+4] 195.0 > 114.0; citrate [M+5] 196.0 > 115.0; citrate [M+6] 197.0 > 116.0. Collision energies and radio frequency (RF) lens voltages were generated for each species using the TSQ Quantiva optimization function.

Mitochondrial respiration measurements were performed in circulating monocytes isolated from pre and post-operative blood samples using the Histopaque method. [18] Oxygen consumption (OCR) and extracellular acidification rates (ECAR) were measured in the absence or presence of 4µM oligomycin, 2µM FCCP or 2µM rotenone and 2µM antimycin A

(Merck, UK) with Seahorse XFe24 analyzer (Agilent Technologies, USA) in 200,000 cells/well. To assess the effect of multimorbidity on glycolysis, OCR was measured in the presence of glucose or pyruvate as substrates. The respiratory control ratio was calculated as described in Hill et al.: RCR_{max}=(FCCP-Antimycin)/(Oligomycin-Antimycin); RCR_{basal}=(Basal-Antimycin)/(Basal-Antimycin) [19]

Cytokine and chemokine panel was assessed by measuring a panel of 71 cytokines/chemokines in plasma samples collected before and 24 hr after surgery by Eve Technologies (Canada). All included samples passed quality control.

Immunohistochemistry was performed on cardiac biopsies. Tissue samples were frozen in OCT (Cell Path, UK) and sliced using Leica CM1520 cryostat (Leica Microsystems, UK) at 10-micron thickness. The slices were fixed in 10% neutral buffered formalin (Merck, UK) and permeabilized in ethanol (50%, 70%, and 100% EtOH). Unspecific binding was blocked with 1% BSA (Merck, UK). Samples were labelled with primary antibodies against nucleolin (rabbit polyclonal, abcam, UK), fibrillarin (rabbit polyclonal, abcam, UK), γH2AX (rabbit polyclonal, abcam, UK) or cardiac troponin T (mouse clone 1C11, abcam, UK). All primary antibodies were used at 1:300 dilution in Co-Detection Antibody Diluent (Advanced Cell Diagnostics, USA). The primary antibodies were detected with secondary Alexa Fluor 568 goat-anti-rabbit (Invitrogen, UK) and Alexa Fluor 488 goat-anti-mouse (Invitrogen, UK) antibodies at 1:200 dilution. Nuclei were labeled with DAPI (Thermo Fisher Scientific, UK). The sections were treated with Prolong Gold Anti-fade media (Invitrogen, UK), and visualized using an inverted Zeiss Axio Observer Z1 microscope equipped with Colibri 2 LED illumination and Plan-Apochromat 63x/1.40 oil objective. For each patient's sample, three slices were prepared and approximately 20 images were collected per slice (400 – 500 cells). Images were analyzed using FIJI ImageJ distribution. [20] Only nuclear fraction of nucleolin staining and nuclear fibrillarin-positive particles were considered in the analysis.

Quantitative real-time PCR to estimate ribosomal DNA (rDNA) copy numbers. The genomic DNA was extracted from cardiac biopsies using a commercial kit following the manufacturer's instructions (Genomic-tip 20/G and Genomic DNA Buffer Set, QIAGEN, UK). Specific primers for amplification of 5S, 5.8S, 18S, and 28S rDNAs were designed using NIH Primer-BLAST tool [21] and synthesized by Merck (UK). As an endogenous PCR control, primers for the β-2-Microglobulin (B2M) gene were used. Primer sequences: rDNA 5S forward TCGTCTGATCTCGGAAGCTAA, reverse AAGCCTACAGCACCCGGTAT; rDNA 5.8S forward GAGGCAACCCCCTCTCCTCTT, reverse: GAGCCGAGTGATCCACCGCTA; rDNA 18S forward:

AGCCTGAGAAACGGCTACCA, reverse: GGTCGGGAGTGGGTAATTTGC; rDNA 28S forward: CTCCGAGACGCGACCTCAGAT, reverse: CGGGTCTTCCGTACGCCACAT;
B2M forward primer TGCTGTCTCCATGTTTGATGTATCT, reverse primer TCTCTGCTCCCCACCTCTAAGT. For each 20µl PCR reaction, 6ng of genomic DNA was combined with 10µl of PowerUp SYBR Green Master Mix (Thermo Fisher Scientific, UK), 1µl of specific primers at 10µM, and nuclease-free water. All reactions were set up in triplicates and measured using a Rotor-Gene Q qPCR machine (Qiagen, UK). Melt curves were produced for all measurements to confirm the presence of a single PCR product. The data were analyzed using the Rotor-Gene Q 2.1.0.9 software (Qiagen, UK).

In vitro experiments

For the estimation of apoptosis and necrosis levels, HL-1 cells (Merck, UK) were grown in 24-well plates and transfected with RPL3 or control siRNA and Lipofectamine RNAiMAX (Thermo Fisher, UK) following the manufacturer's recommendations. The cells were detached from wells with trypsin and labelled with annexin V-FITC (ThermoFisher, UK) or 7-AAD (abcam, UK). The analysis was performed by flow cytometry using CytoFLEX (Beckman Coulter, USA).

For the estimation of apoptosis, cells were plated on Seahorse 24-well plates and transfected as above. Respiration was measured using Seahorse XFe24 analyzer, as described above, without mitochondrial toxins. After the experiments, cells were counted in each well to adjust OCR and ECAR.

RPL3 expression levels were assessed with polyclonal rabbit antibodies against RPL3 (abcam, UK) and rabbit polyclonal antibodies against α-tubulin (abcam, UK) in Western blotting following 12% SDS-PAGE gels.

Data processing and statistical analysis

Unless indicated otherwise, data analysis was performed with R Statistical Computing software version 4.2.2 and plots were prepared with ggplot2 R package. [22,23]

Transcriptomics Sequencing data were quality-checked with Fastqc v0.11.5, [24] quantified with Salmon v1.21 [25] after indexing with a decoy and annotated with Ensembl v100. Gene quantities were normalized to length-scaled transcripts per million and filtered for low quantities before downstream analysis using limma-voom model [26] with empirical Bayes moderation. [27] Sample groups were analyzed with the sequencing batch added to the model as a variable. The false discovery rate was set at 5%. Interactions within networks were visualized with Cytoscape. [28]

Weighted gene correlation network analysis [29] was carried out to cluster differential genes into smaller modules with the soft r-squared set at >0.8 and grey modules excluded. Each module formed was subsetted from the adjacency matrix and exported as edge files for visualization in Cytoscape.

To directly analyze the well-known signalling pathways in the data, a gene-set analysis was carried out on the filtered transcriptome data using camera [30] with Reactome [31] and Gene Ontology [32] annotations for transcripts and non-coding RNA, respectively, with false discovery rate set at 5%.

Metabolomics Untargeted metabolomic profiles were processed by Metabolome Inc. For targeted metabolite analysis, peak area ratio of metabolites was obtained by integration within vendor software (Xcalibur QuanBrowser, Thermo Scientific, Hemel Hempstead, UK) and compared with isotopically labelled standards for quantification. Data were pre-processed by removing constant-value features, replacing zeros and missing values with half the smallest value in the entire dataset and removing extremely low relative standard deviation using Metaboanalyst v5.0. [33] The processed data was log-transformed and mean-normalized. Pairwise comparisons of sample groups were carried out using a t-test. Metabolite set enrichment analysis was performed with Metaboanalyst v5.0.

Multiomics analyses

RNA and metabolite were combined using sparse Partial Least Squares (sPLS) models using mixOmics version 6.22.0. [34] Canonical correlation patterns and association networks derived from the components were then used to infer the relationship between genes and metabolites. The network analysis was visualized with Cytoscape.

Data Availability

Sequencing data are available via NCBI Gene Expression Omnibus (GSE159612). Metabolomics data are available through EMBL-EBI (MTBLS7259).

Results

Study cohort

Out of 1,021 screened patients, 151 were recruited for this study. The reasons for the excluded patients are detailed in **Figure 1A**. From the included patients, six patients have withdrawn from the study, and one patient was excluded for protocol deviation. Data from 144 patients were analyzed.

Multimorbidity was defined as the presence of two or more of nineteen chronic conditions (**Table 1**). Ninety-eight patients suffered from at least two comorbidities (**Figure 1A**). The number of comorbidities per patient ranged between none (11 patients) and seven (three patients) and peaked at two comorbidities per patient (N=48, **Figure 1B**). The most common comorbidity was angina or previous myocardial infarction (**Figure 1B-C**). The incidence of hypertension, angina/MI, heart failure, extracardiac arteriopathy, diabetes, obesity, chronic pulmonary disease and anemia was significantly higher in the multimorbid group.

Patients in the multimorbid group were heavier (BMI 29 vs 28), more often on antidiabetic medications and had increased levels of white blood cells, particularly neutrophils. There were also more patients with NYHA class II, III and IV and CCS angina grades II–IV. Apart from increased lactate levels in the multimorbid patients post-surgery, there was no difference between the groups. However, 11 out of 12 AKI cases were in the multimorbid group (**Table 2**), and PiO2/FiO2 ratio was significantly lower 24, 72 and 96 hrs after surgery (**Figure 1D**). Further correlation analysis indicated that hemoglobin, white blood cell, eosinophils and basophil counts were positively correlated with the number of comorbidities before surgery. Post-surgery, basophil and platelet counts, and lactate were positively correlated with the number of comorbidities, while PiO_2/FiO_2 after return to CICU was correlated negatively.

Analysis of the metabolome was performed in 30 sequential patients. Measurements of transcriptome and metabolites involved in energy production were performed in 53 and 57 sequential patients, respectively. Mitochondrial function in circulating monocytes was performed in 63 sequential patients. The validation included analysis of senescence-associated secretory phenotype, estimations of ribosomal DNA copy numbers (N = 48), DNA damage and nucleolar structure were performed in samples from 29 – 35 patients (**Figure 1A**).

Metabolites analysis

Untargeted metabolomics was performed in myocardial biopsies and pre and post-surgery plasma samples. Myocardial biopsies from four patients were of insufficient quantity (<30 mg) and were not included in the analysis.

The myocardial biopsy dataset comprises 919 compounds, 820 of known identity and 99 of unknown structural identity. The plasma dataset comprises 1316 compounds, 1046 of known identity and 270 of unknown structural identity (**Figure S1A-B**). All samples were comparable in numbers of known, unknown and undetected metabolites (**Figure S1A**). The most numerous metabolites were lipids (376 in biopsies and 483 in plasma), followed by amino acids (164 in biopsies and 216 in plasma, **Figure S1B**). There was no difference in the number of detected myocardial metabolites and their average peak area between patients with multimorbidity and without. That was also true for metabolites in post-operative plasma. However, the number of metabolites detected in pre-operative plasma was significantly higher in multimorbid patients (**Figure S1C**).

The multimorbid samples did not separate well in the principal component analysis. The smallest overlap between the groups was apparent pre-operatively. The greatest effect on global metabolite expression had the surgery (pre vs post-surgery). Biopsy sample 8 and pre-operative plasma sample 3 appeared as outliers (> mean_{Dim2} + 3xSD) and were removed from the analysis (**Figure 2A**).

Since there were no metabolites that passed the false discovery rate adjustment, we performed metabolite set enrichment analysis. Caffeine and vitamin K metabolism and homocysteine degradation pathways were significantly enriched in myocardial biopsies. Caffeine metabolism was also significantly enriched in pre and post-operative plasma. Amino-acid metabolism pathways, ketone metabolism and malate-aspartate shuttle pathways were among the most significantly enriched in pre-operative plasma, suggesting dysregulation of energy production. In addition to caffeine metabolism, metabolites from post-operative plasma enriched threonine and oxobutanoate degradation, as well as purine, selenoamino acid and propanoate metabolism pathways (**Figure 2B** and **Tables S2-S4**). In the myocardial biopsies, hercynine was most downregulated, and S-(1,2-dicarboxyethyl)glutathione was most upregulated. In pre-operative plasma 3-hydroxybutyrate (BHBA) and oleoyltaurine were most downregulated, and glycocholate and 3-methoxycatechol sulfate were most upregulated. In post-operative plasma, ergothioneine was most downregulated, and 3-methoxytyramine sulfate was most upregulated. Metabolites significantly different in at least two types of samples are shown in **Figure 2C**.

The most upregulated metabolites in at least two types of samples were sulfated steroids and caffeine breakdown products.

To assess similarities between multimorbidity and single comorbidities, we performed Euclidean hierarchical clustering using fold change of metabolites significantly different for miltimorbidity and each comorbidity. **Figure 2D** shows that multimorbidity has a distinct profile of differentially expressed metabolites (highlighted green in **Tables S2 – S4**). These included fucose, oxidized and S-(1,2-dicarboxyethyl)-glutathione or hexanoylcarnitine in biopsies. Amino acids (N=19) and lipids (N=15) with several species of long-chain acyl-glycerophosphoethanolamine dominated in pre-operative plasma. The specific metabolites in the post-operative plasma were also mainly amino acids and lipids with several sphingomyelin species. Metabolites involved in caffeine metabolism correlated positively with the number of comorbidities in all three types of samples (**Tables S2 – S4**).

Transcripts analysis

The transcriptomics analysis was performed on myocardial biopsies and summary of the dataset is published elsewhere. [35] Multimorbidity did not have a major effect on gene expression patterns, as indicated by the principal component analysis (**Figure 3A**). However, comparisons with significant transcripts in all analyzable comorbidities indicated a specific multimorbid transcript profile (**Figure 3B** and highlighted green in **Table S5**). The differential expression analysis detected 854 transcripts (**Table S5**). Most upregulated transcripts encoded immunoglobulin chains. Three hundred forty-three transcripts were specific to multimorbid samples (highlighted green in **Table S5**).

Since none of the transcripts passed the multiple comparison adjustment, we first performed a weighted gene correlation analysis to identify significantly changing groups of transcripts. The analysis identified one network of transcripts that was significantly downregulated (blue in **Figure 3C, D**) in the multimorbid myocardium and three significantly upregulated networks (brown, turquoise and yellow in **Figure 3C, D**). The grey network annotation in **Table S5** includes transcripts without network membership. The blue network included transcripts that enriched pathways involved in mitochondrial oxidative respiration, mitochondrial biogenesis, mitophagy and amino acids metabolism. It included, among others, NUDS1 NUDV2, PDHB, OGHD. The brown network's transcripts significantly enriched pathways involved in DNA damage processing and packaging, senescence, translation and regulation of ribosomal RNA expression. The transcripts included in this network were mainly ribosomal proteins, histone 2B and histone ubiquitin ligases. The turquoise and yellow networks included transcripts that significantly enriched innate immunity pathways.

It included proteins required for neutrophil degranulation (LAMP1, PYCARD, FTL or RAB5C) but also proteins modulating inflammatory response like serpins (A1, B1, E2, F1 and H1) and anti-apoptotic proteins like S100 (A4, A8, A9 and A11) or HMOX1. Transcripts membership in each network is indicated in **Table S5,** and pathway enrichment results are in **Table S6**.

Finally, we performed gene set enrichment analysis using the whole gene expression dataset (**Table S7**). The bar plot in **Figure 3E** shows pathways specific to multimorbidity. Diagrams in the left panel show transcripts annotated to and linked by joint pathway membership. The significant transcripts involved in the enriched pathways mainly encode proteins regulating chromatin condensation: Ubiquitin-60S ribosomal protein L40 (UBA52), E3 ubiquitin-protein ligases RNF40, RNF8 and ANAPC15, Protein arginine N-methyltransferase 1 (PRMT1), Bromodomain-containing protein 8 (BRD8) and Serine/threonine-protein kinase greatwall (MASTL), Repressor methyl-CpG-binding domain protein 2 (MBD2), Chromobox protein homolog 3 (CBX3), Structural maintenance of chromosomes protein 2 (SMC2), Mastermind-like protein 1 (MAML1); transcripts involved in gene transcription and polymerase I-interacting proteins: DNA-directed RNA polymerase I subunit RPA1 (POLR1A), Homeodomain-containing DNA binding protein 3 (HOXB3); and transcripts encoding nuclear export and cytoskeletal proteins: Exportin-5 (XPO5), Myosin-14 (MYH14), Myosin light polypeptide 6 (MYL6), Nesprin-1 (SYNE1). The only downregulated pathway was the utilization of ketone bodies with two significantly downregulated transcripts: Succinyl-CoA:3-ketoacid coenzyme A transferase 1 (OXCT1) and D-β-hydroxybutyrate dehydrogenase (BDH1).

Respiration in circulating monocytes

Our attempts to measure respiration in myocardial biopsies were very variable within technical repeats and unreliable. In addition, disintegration or tissue homogenization can result in clinically irrelevant data. Therefore, we measured respiration in circulating monocytes as a proxy for the myocardium. In contrast to granulocytes, monocytes depend on oxidative phosphorylation for energy production and are considered a good sensor for metabolic stressors. [36]

The analysis of oxygen consumption rate (OCR) identified pre-operative basal (without any drugs) and maximal (in the presence of FCCP) respiratory control ratios (RCR) as significantly downregulated in the multimorbid samples. No difference in monocytic mitochondrial respiration was observed after surgery. The RCR is a measure of mitochondrial coupling (see Material and Methods for definitions) , which links respiration to ATP synthesis. However, the RCR component measurements were not different between the

groups. Therefore, we analyzed correlations of the number of comorbidities with OCR measurements. Significant correlations were found with baseline OCR and basal RCR, indicating that pre-operative basal respiration is likely the most affected parameter by the accumulating comorbidities.

The analysis of extracellular acidification rate (ECAR), which is a measure proportional to glycolysis, did not find any significant differences (**Figure 4D**). To further test the role of glycolysis, we measured the difference in maximal OCR in the presence of glucose (glycolysis substrate) and pyruvate (glycolysis product). There was no difference in that measure, as well (**Figure 4A**, $Maximal_{Pyr}$-$Maximal_{Glucose}$).

A comparison of OCR between comorbidities and multimorbidity is presented in **Figure 4E**. Maximal RCR was also downregulated in renal disease. This comorbidity affects mitochondrial respiration to the highest degree, as maximal respiration and spare capacity were also downregulated pre-surgery. Post-surgery, mitochondrial function was most affected in people with arthritis, where the spare capacity was reduced and basal and ATP-linked OCR increased.

Comparison of ECAR between comorbidities suggested that glycolysis is most downregulated in people with renal disease both before and after surgery. On the other hand, people with extracardiac arteriopathy have increased levels of ECAR after surgery (**Figure 5F**).

Energy metabolism in multimorbidity

The above analyses indicated that mitochondrial function is affected by multimorbidity. Since we could not measure respiration in the myocardial biopsies, we analyzed a set of metabolites involved in energy metabolism. Out of 144 metabolites, ten metabolites and one metabolite ratio were significantly different in the multimorbid myocardium. That included α-ketoglutarate, ATP, UTP, long-chain acyl-carnitines formyl-valine and $NADH/NAD^+$ ratio (**Figure 5A**). Further correlation analysis confirmed the role of α-ketoglutarate, ATP, UTP and formyl-valine, whose levels decreased with the number of comorbidities. On the other hand, NADH/NAD+ ratio increased with the number of comorbidities. In addition, the analysis identified cytosine, cytidine, hydroxylated and stearoylcarnitine (C18-OH) as positively correlated, and asymmetric dimethylarginine (ADMA) as negatively correlated with the number of comorbidities (**Figure 5B**).

The metabolites significant in groupwise comparisons and correlation analysis were combined with paired transcriptomics in weighted gene correlation analysis using correlation cutoffs above and below 0.6 and -0.6, respectively. The three long-chain acyl-

carnitines (C18:1, C18:2 and C16:1) positively correlated mainly with transcripts involved in the citric acid cycle and respiratory electron transport chain: NUDS1 NUDV2, PDHB, OGHD, COQ10A, ACO2, SUCLA2, NNT, PDHX, SDHA, VDAC1 but also with solute carrier SLC2A4 and heart-specific ribosomal protein RPL3L. A negative correlation was found between Guanine nucleotide-binding protein subunit gamma-12 (GNG12), Microfibril-associated glycoprotein 4 (MFAP4) and Transmembrane protein 176A (TMEM176A). ATP and UTP correlated negatively with TMEM176A and Collagen α-1(XXIII) chain (**Figure 5C**).

Senescence-associated secretory phenotype

Transcript analysis identified changes in processes and pathways that are associated with senescence, including mitochondrial oxidative respiration, mitochondrial biogenesis, inflammation, mitophagy, DNA damage processing and packaging. Moreover, transcripts like IGFBP7 (**Figure 3C**), TIMP1, collagen, laminin, CCL13 and C-C/C-X-C chemokines receptors (**Table S4**), showing differential regulation in the multimorbid myocardial samples, encode proteins whose expression changes in senescence and are part of the senescence-associated secretory phenotype (SASP). [37,38]

Therefore, we tested whether cytokines previously described as SASP proteins were upregulated in the pre-operative plasma samples. To do this, we analyzed a panel of 71 cytokines and chemokines in samples from 48 patients. The panel includes cytokines that are regulated by NF-κB or IL-1/NLRP3, which are major modulators and initiators of SASP expression. [39,40]

Groupwise comparison indicated that fractalkine and IL-22 were significantly upregulated in the multimorbid samples (**Figure 6A**). Further correlation analysis with the number of comorbidities added GM-CSF, IL-1β, IL-1RA and IL-3 to the list (**Figure 6B**). Comparison of cytokine profiles between multimorbidity and single comorbidities indicated that only IL-22 was specifically upregulated in multimorbidity (**Figure 6C**)

DNA damage and nucleolar assembly

Transcriptomics data suggested that the primary driver of senescence, DNA damage repair is upregulated in multimorbidity. In addition, several transcripts encoding ribosomal proteins and others involved in polymerase I transcription and ribosomal RNA processing were affected (**Figure 3C**). This can indicate dysregulation of nucleolar assembly, which can result in free ribosomal proteins, increased senescence levels and, consequently, changes in mitochondrial respiration. [41]

We first tested ribosomal DNA (rDNA) copy numbers, as it was previously linked with mitochondrial abundance. [42] We analyzed rDNA in myocardial biopsies with qRT-PCR and

specific primers, and as shown in **Figure 7A**; however, we did not detect any difference in rDNA copy numbers between the groups. DNA damage was detected with antibodies against the phosphorylated form of histone 2AX (γH2AX) in myocardial cryo-slices. Multimorbid samples had significantly more nuclei positive for γH2AX (**Figure 7B, C**). Next, the nucleolar stress was tested with antibodies against nucleolin and fibrillarin. Although fibrillarin staining patterns were not different in multimorbid samples, nucleolin labelling indicated higher levels of nucleolar stress as indicated by a larger fraction of nuclear area positive for nucleolin (**Figure 7D – F**).

Nucleolus is responsible for ribosomal assembly, and our transcriptomics analysis suggest that several ribosomal proteins are upregulated. Dysregulation of ribosomal assembly can lead to changes that affect mitochondrial function. To test this connection, we silenced RPL3 in murine cardiomyocyte cell line HL-1. Downregulation of RPL3 ranged from 20 – 80% in our experiments (**Figure 7G**) and did not result in increased levels of apoptosis or necrosis (annexin V and 7-AAD staining, respectively in **Figure 7H**). However, RPL3 silencing significantly reduced levels of basal oxygen consumption rate (**Figure 7I**). The extracellular acidification rate was not significantly affected although it was apparently reduced (**Figure 7J**).

Discussion

Multimorbidity is manifested by distinct metabolomics and transcriptomics profiles in myocardial tissue and plasma. The analysis of these profiles suggested dysregulation of mitochondrial function, which was corroborated by increased basal respiration levels in circulating monocytes and significantly decreased levels of several species of long-chain acylcarnitines in the myocardial tissue. The acylcarnitines correlated with transcripts encoding proteins with a function in the citric acid cycle and mitochondrial electron transport chain. The transcriptomics analysis further pointed towards dysregulation of epigenetic regulation of gene expression, increased DNA damage and nucleolar stress. The changes in the gene expression patterns are similar to changes characteristic of cellular senescence. Indeed, IL-1β, its receptor and fractalkine correlated positively with the number of comorbidities. The further independent analysis confirmed higher levels of DNA damage and nucleolar stress in the multimorbid samples.

We adopted the most common definition of multimorbidity, two or more coexisting chronic conditions where at least one is physical. [43] That is also the consensus reached by professional and public panels and is most often used in the literature. [44,45] An alternative definition is a coexistence of three, five or more chronic conditions, or 'complex multimorbidity'. The latter is the co-occurrence of three or more chronic conditions affecting three or more different body systems within one person. [46,47] However, the alternative definitions are used less frequently in the literature, and the 'complex multimorbidity' definition was used only in three reports. [45] To define multimorbidity, we used a simple count of comorbidities, which is also the most common approach in the literature [46] and preferred by professional and public panels [44] That is in contrast to using weighted indices for risk adjustment and prediction of comorbidities' outcomes. The limitation of this study is that all considered comorbidities were physical, as we did not have information about chronic psychological conditions. Several comorbidities were significantly enriched in the multimorbid groups (**Table 1**) and could potentially influence the results. However, multimorbidity had metabolite and transcripts expression profiles distinct from any significant comorbidities. Multimorbidity was most similar to angina or previous myocardial infarction, which was present in nearly 50% of patients with multimorbidity. However, angina/MI mainly affected native immunity pathways, not DNA repair, translation or senescence.

The patient cohort used in this study was of low risk, which is indicated by the fact that over 80% of patients had two or fewer comorbidities. That can explain the low incidence of

short-term adverse outcomes after surgery. Nevertheless, the lung function was significantly affected, and lactate levels raised significantly after surgery. In addition, nearly all AKI cases were in the multimorbid group. Multimorbid patients had higher granulocyte counts that also correlated with the number of comorbidities. That can indicate higher levels of activity in the innate immune system, which is often increased in chronic conditions [48] (**Table S7**). The limitation of this study is that we did not collect information about long-term mortality and adverse events.

Our transcriptomics analysis could distinguish three major processes that are affected by multimorbidity. These are innate inflammation (turquoise and yellow networks), epigenetic regulation of gene expression and DNA repair (brown network) and mitochondrial energy production (blue network). While the inflammatory processes appear common in many of the included comorbidities, some aspects of mitochondrial function and epigenetic regulation are specific to multimorbidity. The epigenetic pathways concentrate on histone modifications, as the expression of histone 2B (H2B) and its E3 ubiquitin ligase (RNF40), as well as several other ubiquitin ligases, were increased in the multimorbid group. H2B ubiquitynation on K120 is known to stimulate rapid changes in chromatin remodeling and transcriptional activity. Minsky et al. showed that the upregulation of p53, a transcription factor involved in senescence, correlates with H2B ubiquitination of the region encoding p21, a p53 target gene. [49] Although we did not observe upregulation of CDKN1A (human p21 orthologue), several genes regulated by TP53 (human p53 orthologue) were affected. These include IGFBP7, TAB3 (TGF-β-activated kinase 1), AKT3 (RAC-gamma serine/threonine-protein kinase), ANAPC15, GNG12 (G protein subunit gamma 12). [50] That indicates senescence-like transcriptional changes, which are further supported by higher levels of DNA damage and potential activation of PI3K/AKT/mTOR pathway, as indicated by increased levels of AKIT3. All these processses are activated in accelerated aging. [48,51] As a consequence of the above changes, the nucleolus becomes destabilized with potential defects in ribosomal assembly. That leads to free ribosomal proteins that affect other processes. For example, ribosomal proteins L23, L29, S3 and S15 (upregulated in our dataset) bind MDM2, a TP53 ubiquitin ligase, enabling senescence-specific gene expression. [41] Free nuclear RPS3 binds to oxidative lesions in DNA and inhibits DNA repair, [52] and RPL3 upregulates CDKN1A inducing mitochondrial-driven apoptosis.[34] Interestingly, the expression of mitochondrial ribosomal proteins was lower in the multimorbid group. The changes in the expression of ribosomal proteins are subtle, and it is hard to speculate whether they are responsible for changes in the mitochondrial function in in the multimorbid myocardium. However,

decreased basal mitochondrial respiration after silencing RPL3 in HL-cells indicates a type of cross-signaling between the expression of ribosomal proteins and mitochondrial function. Moreover, expression of heart-specific RPL3L positively correlated with decreased expression of acylcarnitines in the myocardium.

The multimorbid group had increased levels of oxidized glutathione and lower levels of antioxidants like ergothioneine and hercynine. [53] That together with higher levels of γH2AX (a marker of DNA damage), can suggest oxidative stress. However, we did not detect any 8-hydroxy-2'-deoxyguanosine in plasma of patients with multimorbidity; therefore, we suspect that the multimorbid patients suffer only mild oxidative imbalance. The most likely explanation for the imbalance is the activation of the immune response, which is prominent in multimorbidity and nearly all included comorbidities. Oxidative stress can lead to activation of PI3K/AKT/mTOR pathway, which downregulates DNA repair response, aggravates mitochondrial defects, and triggers senescence-associated secretory phenotype. [48]

We suspect that senescence was activated to a degree, as discussed above. However, analysis of cytokines and chemokines detected only IL-1β, IL-1RA and GM-CSF that are known members of the senescence-associated phenotype. [37] These analytes correlated positively with the number of comorbidities in our dataset. Fractalkine, whose levels drop with senolytic treatments, [38] and can be indicative of heart failure, [52] also increased in the multimorbid group. However, levels of these analytes were also higher in anemia, chronic pulmonary disease, hypertension and stroke. The only analyte specific to multimorbidity was IL-22, which is secreted by T cells, promotes survival, inhibits apoptosis and induces expression of pro-survival molecules like S100. [54] That effect is most likely the consequence of the elevated immune response, as S100 proteins clustered together with other neutrophil degranulation proteins, which are potentially expressed by the myocardial immune cell population, which is indistinguishable in bulk sequencing.

An intriguing observation is a change in caffeine metabolism: caffeine and its breakdown products accumulated in heart tissue and plasma before and after surgery. It is normally broken down in the liver's endoplasmic reticulum by cytochrome p450 enzymes, followed by further processing in lysosomes before secretion in urine. The effect could be a consequence of a changed NADH/NAD^+ ratio, which can influence the activity of cytochrome p450 enzymes and, consequently, oxidation of fatty acids and steroids, whose expression changes plasma. Cytochrome p450 enzymes are often affected in polypharmacy, [55] closely associated with multimorbidity.

We realize that the transcriptomics and particularly untargeted metabolomics analyses may not have been adequately powered due to heterogeneity between patients and budgetary limitations. In addition, myocardial biopsies may not have been uniform in cell content and included fragments of blood vessels or fat tissue, which further adds to the heterogeneity between samples. Due to the small sizes of the biopsies, it was impossible to estimate the variation in the cell composition. However, fluorescent image analysis indicates that most cells were cardiomyocytes, as expected. Finally, due to the limited material availability, we could not perform all analyses on all samples.

In conclusion, our data suggest that accumulating comorbidities elevate innate immune response that leads to oxidative stress responsible for DNA damage and epigenetic changes that trigger senescence-like gene expression. Thst can potentially happen through PI3K/AKT/mTOR pathway. The DNA damage and epigenetic changes affect nucleolar function and ribosomal assembly followed by changes in the mitochondrial function. The latter can, in turn, aggravate oxidative stress and senescence [56] and result in higher susceptibility to insults like cardiac surgery. Our results suggest that drugs like metformin or rapamycin modulating mTOR could be effective in reversing DNA damage and unfavourable epigenetic changes in patients with multimorbidity to prevent adverse outcomes after surgery. Alternatively, anti-inflammatory drugs like colchicine may effectively prevent the buildup of innate immune cells in tissues and local oxidative stress.

Funding

This work was supported by Van Geest Foundation, Leicester NIHR Biomedical Research Centre, British Heart Foundation [CH/12/1/29419, AA18/3/34220].

Author Contribution Statement

Individual contributions to the study were as follows: MJW and GJM designed the study; MJW, TK and MR wrote the manuscript and prepared tables and figures; MR, HA, BA and LJ-D managed the conduct of the study; FYL, MR, HA and LJ-D managed the data during the study; TK, MR, LJ-D, SY, BE-H and SS collected samples and undertook the laboratory analyses; MG, AM and JLG performed targeted metabolite analysis. MJW and FYL carried out statistical analyses; MJW and ASA performed bioinformatics analyses. GDR shared experimental protocols and contributed to paper writing. All authors reviewed the report for important intellectual content and approved the final version.

Conflict of Interest

Prof. Murphy received grants from Terumo and Baxter. The remaining authors have disclosed that they do not have any potential conflicts of interest.

References

1. Theou, O., Rockwood, M. R. H., Mitnitski, A. & Rockwood, K. Disability and co-morbidity in relation to frailty: how much do they overlap? *Arch Gerontol Geriatr* **55**, e1-8 (2012).
2. Fortin, M., Soubhi, H., Hudon, C., Bayliss, E. A. & van den Akker, M. Multimorbidity's many challenges. *BMJ* **334**, 1016–1017 (2007).
3. Kingston, A. *et al.* Projections of multi-morbidity in the older population in England to 2035: estimates from the Population Ageing and Care Simulation (PACSim) model. *Age Ageing* **47**, 374–380 (2018).
4. Barnett, K. *et al.* Epidemiology of multimorbidity and implications for health care, research, and medical education: a cross-sectional study. *Lancet* **380**, 37–43 (2012).
5. Forman, D. E. *et al.* Multimorbidity in Older Adults With Cardiovascular Disease. *J Am Coll Cardiol* **71**, 2149–2161 (2018).
6. Stirland, L. E. *et al.* Measuring multimorbidity beyond counting diseases: systematic review of community and population studies and guide to index choice. *BMJ* **368**, m160 (2020).
7. Haug, N. *et al.* High-risk multimorbidity patterns on the road to cardiovascular mortality. *BMC Medicine* **18**, 44 (2020).
8. Hassaine, A., Salimi-Khorshidi, G., Canoy, D. & Rahimi, K. Untangling the complexity of multimorbidity with machine learning. *Mech Ageing Dev* **190**, 111325 (2020).
9. Kameda, M., Teruya, T., Yanagida, M. & Kondoh, H. Frailty markers comprise blood metabolites involved in antioxidation, cognition, and mobility. *Proc Natl Acad Sci U S A* **117**, 9483–9489 (2020).
10. Kemp, P. R. *et al.* Metabolic profiling shows pre-existing mitochondrial dysfunction contributes to muscle loss in a model of ICU-acquired weakness. *J Cachexia Sarcopenia Muscle* **11**, 1321–1335 (2020).
11. Rattray, N. J. W. *et al.* Metabolic dysregulation in vitamin E and carnitine shuttle energy mechanisms associate with human frailty. *Nat Commun* **10**, 5027 (2019).
12. von Elm, E. *et al.* The Strengthening the Reporting of Observational Studies in Epidemiology (STROBE) statement: guidelines for reporting observational studies. *J Clin Epidemiol* **61**, 344–349 (2008).
13. Kidney Disease: Improving Global Outcomes (KDIGO) CKD Work Group. KDIGO 2012 Clinical Practice Guideline for the Evaluation and Management of Chronic Kidney Disease. *Kidney inter. Suppl.* **3**, 1–150 (2013).

14. Plagg, B., Ehrlich, D., Kniewallner, K. M., Marksteiner, J. & Humpel, C. Increased Acetylation of Histone H4 at Lysine 12 (H4K12) in Monocytes of Transgenic Alzheimer's Mice and in Human Patients. *Curr Alzheimer Res* **12**, 752–760 (2015).
15. Jin, L. *et al.* Genomewide Histone H3 Lysine 9 Acetylation Profiling in CD4+ T Cells Revealed Endoplasmic Reticulum Stress Deficiency in Patients with Acute-on-chronic Liver Failure. *Scand J Immunol* **82**, 452–459 (2015).
16. Charidemou, E. *et al.* A randomized 3-way crossover study indicates that high-protein feeding induces de novo lipogenesis in healthy humans. *JCI Insight* **4**, e124819, 124819 (2019).
17. West, J. A. *et al.* A targeted metabolomics assay for cardiac metabolism and demonstration using a mouse model of dilated cardiomyopathy. *Metabolomics* **12**, 59 (2016).
18. Köhler, W. N. R. Rose and H. Friedman (Editors), Manual of Clinical Immunology. 932 S., 192 Abb., 151 Tab. Washington 1976: American Society for Microbiology. $ 20.00. *Zeitschrift für allgemeine Mikrobiologie* **17**, 578–578 (1977).
19. Hill, B. G. *et al.* Integration of cellular bioenergetics with mitochondrial quality control and autophagy. *Biol Chem* **393**, 1485–1512 (2012).
20. Schindelin, J. *et al.* Fiji: an open-source platform for biological-image analysis. *Nat Methods* **9**, 676–682 (2012).
21. Ye, J. *et al.* Primer-BLAST: A tool to design target-specific primers for polymerase chain reaction. *BMC Bioinformatics* **13**, 134 (2012).
22. R Core Team. R: A language and environment for statistical computing. R Foundation for Statistical Computing. (2022).
23. Wickham, H. *ggplot2: Elegant Graphics for Data Analysis*. (Springer, 2009). doi:10.1007/978-0-387-98141-3.
24. Wingett, S. W. & Andrews, S. FastQ Screen: A tool for multi-genome mapping and quality control. *F1000Res* **7**, 1338 (2018).
25. Patro, R., Duggal, G., Love, M. I., Irizarry, R. A. & Kingsford, C. Salmon provides fast and bias-aware quantification of transcript expression. *Nat Methods* **14**, 417–419 (2017).
26. Ritchie, M. E. *et al.* limma powers differential expression analyses for RNA-sequencing and microarray studies. *Nucleic Acids Res* **43**, e47 (2015).
27. McCarthy, D. J., Chen, Y. & Smyth, G. K. Differential expression analysis of multifactor RNA-Seq experiments with respect to biological variation. *Nucleic Acids Res* **40**, 4288–4297 (2012).

28. Shannon, P. *et al.* Cytoscape: a software environment for integrated models of biomolecular interaction networks. *Genome Res* **13**, 2498–2504 (2003).
29. Langfelder, P. & Horvath, S. Fast R Functions for Robust Correlations and Hierarchical Clustering. *J Stat Softw* **46**, i11 (2012).
30. Wu, D. & Smyth, G. K. Camera: a competitive gene set test accounting for inter-gene correlation. *Nucleic Acids Research* **40**, e133 (2012).
31. Gillespie, M. *et al.* The reactome pathway knowledgebase 2022. *Nucleic Acids Research* **50**, D687–D692 (2022).
32. Mi, H., Muruganujan, A., Ebert, D., Huang, X. & Thomas, P. D. PANTHER version 14: more genomes, a new PANTHER GO-slim and improvements in enrichment analysis tools. *Nucleic Acids Res* **47**, D419–D426 (2019).
33. Xia, J., Psychogios, N., Young, N. & Wishart, D. S. MetaboAnalyst: a web server for metabolomic data analysis and interpretation. *Nucleic Acids Research* **37**, W652–W660 (2009).
34. Lê Cao, K.-A., Martin, P. G., Robert-Granié, C. & Besse, P. Sparse canonical methods for biological data integration: application to a cross-platform study. *BMC Bioinformatics* **10**, 34 (2009).
35. Adebayo, A. S. *et al.* Gene and metabolite expression dependence on body mass index in human myocardium. *Sci Rep* **12**, 1425 (2022).
36. Kramer, P. A., Ravi, S., Chacko, B., Johnson, M. S. & Darley-Usmar, V. M. A review of the mitochondrial and glycolytic metabolism in human platelets and leukocytes: Implications for their use as bioenergetic biomarkers. *Redox Biol* **2**, 206–210 (2014).
37. Coppé, J.-P., Desprez, P.-Y., Krtolica, A. & Campisi, J. The Senescence-Associated Secretory Phenotype: The Dark Side of Tumor Suppression. *Annu Rev Pathol* **5**, 99–118 (2010).
38. Dookun, E. *et al.* Clearance of senescent cells during cardiac ischemia-reperfusion injury improves recovery. *Aging Cell* **19**, e13249 (2020).
39. Acosta, J. C. *et al.* A complex secretory program orchestrated by the inflammasome controls paracrine senescence. *Nat Cell Biol* **15**, 978–990 (2013).
40. Salminen, A., Kauppinen, A. & Kaarniranta, K. Emerging role of NF-κB signaling in the induction of senescence-associated secretory phenotype (SASP). *Cell Signal* **24**, 835–845 (2012).

41. Wang, W. *et al.* Ribosomal Proteins and Human Diseases: Pathogenesis, Molecular Mechanisms, and Therapeutic Implications. *Medicinal Research Reviews* **35**, 225–285 (2015).
42. Gibbons, J. G., Branco, A. T., Yu, S. & Lemos, B. Ribosomal DNA copy number is coupled with gene expression variation and mitochondrial abundance in humans. *Nat Commun* **5**, 4850 (2014).
43. Quality standard [QS153]. Multimorbidity. https://www.nice.org.uk/guidance/qs153 (2017).
44. Ho, I. S. S. *et al.* Measuring multimorbidity in research: Delphi consensus study. *BMJ Medicine* **1**, (2022).
45. Ho, I. S.-S. *et al.* Examining variation in the measurement of multimorbidity in research: a systematic review of 566 studies. *Lancet Public Health* **6**, e587–e597 (2021).
46. Harrison, C., Britt, H., Miller, G. & Henderson, J. Examining different measures of multimorbidity, using a large prospective cross-sectional study in Australian general practice. *BMJ Open* **4**, e004694 (2014).
47. Skou, S. T. *et al.* Multimorbidity. *Nat Rev Dis Primers* **8**, 48 (2022).
48. Barnes, P. J. Mechanisms of development of multimorbidity in the elderly. *European Respiratory Journal* **45**, 790–806 (2015).
49. Minsky, N. *et al.* Monoubiquitinated H2B is associated with the transcribed region of highly expressed genes in human cells. *Nat Cell Biol* **10**, 483–488 (2008).
50. Fischer, M. Census and evaluation of p53 target genes. *Oncogene* **36**, 3943–3956 (2017).
51. Xu, S., Cai, Y. & Wei, Y. mTOR Signaling from Cellular Senescence to Organismal Aging. *Aging Dis* **5**, 263–273 (2013).
52. Hegde, V., Yadavilli, S. & Deutsch, W., A. Knockdown of ribosomal protein S3 protects human cells from genotoxic stress. *DNA repair* **6**, (2007).
53. Paul, B. D. & Snyder, S. H. The unusual amino acid L-ergothioneine is a physiologic cytoprotectant. *Cell Death Differ* **17**, 1134–1140 (2010).
54. Dudakov, J. A., Hanash, A. M. & van den Brink, M. R. M. Interleukin-22: Immunobiology and Pathology. *Annual Review of Immunology* **33**, 747–785 (2015).
55. Doan, J., Zakrzewski-Jakubiak, H., Roy, J., Turgeon, J. & Tannenbaum, C. Prevalence and Risk of Potential Cytochrome P450–Mediated Drug-Drug Interactions in Older Hospitalized Patients with Polypharmacy. *Ann Pharmacother* **47**, 324–332 (2013).
56. Anderson, R. *et al.* Length-independent telomere damage drives post-mitotic cardiomyocyte senescence. *The EMBO Journal* **38**, e100492 (2019).

Table and Figure legends

Table 1 Distribution of comorbidities between the groups.

Table 2 Patients' characteristics *Tests between the groups were conducted by exact test for categorical variables and t-test or non-parametric Wilcox test for continuous variables. Data is presented as n (%) for categorical variables and mean (standard deviation) or median (interquartile range) for continuous variables.

Figure 1 Cohort characteristics A – CONSORT diagram; **B** – Comorbidities distribution in patients without or with a specific number of comorbidities; **C** – Comorbidities distribution in patients without and with multimorbidity; **D** – PiO_2/FiO_2 ratio before and after surgery.

Figure 2 Metabolite analysis A – Principal component (1 and 2) plots for the detected metabolites in the myocardial biopsies and plasma. **B** – Metabolite set enrichment analysis in myocardial biopsies and plasma samples; the color scale indicates enrichment p-value. **C** – Differentially expressed metabolites in at least two types of samples. Colors indicate the log fold change, where positive numbers indicate upregulation and negative downregulation in the multimorbid group. **D** – Comparison of differentially expressed metabolites between multimorbidity and single comorbidities. Colors indicate the fold change. Metabolites specifically expressed in multimobidity are marked green in Tables S2 – S4.

Figure 3 Transcripts analysis A - Principal component (1 and 2) plots for the myocardial transcriptomics profiles. **B** – Comparison of differentially regulated transcripts between multimorbidity and single comorbidities. Colors indicate the log fold change. Transcripts specifically expressed in multimobidity are marked green in Table S5. **C** – Transcripts networks identified in weighted gene correlation network analysis. Green indicates a negative correlation with the number of comorbidities, and red indicates a positive correlation. The numbers show a correlation estimate (p-value). **D** – Network eigengene values distribution between the groups. Genes constituting each network were subjected to pathway enrichment analysis, and the summary is shown below the plots. The full list of pathways is in Table S6. **E** – Outcome of gene set enrichment analysis. The barplot shows significantly regulated pathways (adjusted p-value<0.05), and the diagrams show transcripts sharing membership in at least one pathway. The node fill color shows transcripts' log fold change with positive numbers indicating upregulation in multimorbidity. The colors in the node edge indicate a number of pathways the transcript participates in.

Figure 4 Mitochondrial respiration in monocytes A – The assays were performed without or with mitochondrial toxins: oligomycin (ATPase synthase inhibitor), FCCP (drug uncoupling ATP synthesis and electron transport), antimycin A (complex III inhibitor) and

rotenone (complex I inhibitor). The summary of the measured OCR parameters is shown in the left panel. The right panel shows the oxygen consumption rate in monocytes before and after surgery. $Maximal_{Pyr}$-$Maximal_{Glucose}$ is the difference between maximal respiration (in the presence of FCCP) in the presence of pyruvate and glucose. **B** – Box plots of the significantly different mitochondrial parameters between multimorbid and non-multimorbid samples. **C** – Plots of mitochondrial parameters significantly correlating with the number of comorbidities. **D** – ECAR in monocytes before and after surgery (left panel) and summary of the measured ECAR parameters. **E** – Comparison of OCR parameters between multimorbidity and single comorbidities. **F** – Comparison of ECAR parameters between multimorbidity and single comorbidities. Colors in E and F indicate log fold change, where positive numbers indicate higher levels in multimorbidity/comorbidity.

Figure 5 Metabolites involved in energy metabolism A – Targeted metabolites significantly different in multimorbid myocardium. B - Targeted metabolites significantly correlating with the number of comorbidities. C - Transcripts and metabolite were combined using sparse Partial Least Squares models with 0.6 cut-off. Node color indicates expression log fold change in the multimorbid group. Red edges show a positive and blue edges show a negative correlation between nodes.

Figure 6 Senescence-associated secretory phenotype A – Boxplots of analytes significantly different in multimorbidity. **B** – Plots of analytes correlating significantly with the number of comorbidities. **C** – comparison of significant analytes in multimorbidity and single comorbidities. The color indicates log fold change in multimorbidity.

Figure 7 DNA damage and nucleolar stress A – Ribosomal DNA copy numbers were analyzed by qRT-PCR with specific primers to genes encoding ribosomal DNA. The CT values were normalised against β-2-Microglobulin. B – γH2AX was detected in cryosections of myocardial biopsies, and the numbers indicating the percentage of γH2AX-positive cells were plotted. C – Representative images of cryosections labelled with γH2AX. D – Nucleolin was detected in cryosection, and the plots show the percentage of nuclear area occupied by the nucleolin staining. E – Representative images after the nucleolin labelling. Scale bars in C and E are 50 µm. F – Fibrillarin was detected in cryosection and plots show the number of nuclear fibrillarin spots. G – RPL3 was silenced as described in Materials and Methods. The expression levels were assessed in three independent experiments with three repeats for RPL3 siRNA within each experiment using specific antibodies against RPL3 normalized against α-tubulin expression. The expression levels are shown as a fraction of RPL3 expression in cells transfected with control siRNA. H – Annexin V and 7AAD staining in cells

transfected with RPL3 and control siRNAs, estimated by flow cytometry. I – Basal oxygen consumption rate in cells transfected with RPL3 and control siRNAs. J – Basal extracellular acidification rate in cells transfected with RPL3 and control siRNAs.

Table 1 Distribution of comorbidities between the groups.

	Multimorbidity				
Comorbidity	**No (n=46)**	**Yes (n=98)**	***p*-value**	**Missing data**	**System**
Cancer	0 (0%)	2 (1.39%)	1	0	Cancer
Stroke (CVA/TIA)	2 (1.39%)	10 (6.94%)	0.339	0	Cardiovascular
Hypertension	0 (0%)	17 (11.81%)	**0.001**	0	Cardiovascular
Angina/MI	13 (9.03%)	71 (49.31%)	**<0.001**	0	Cardiovascular
Hyperlipidemia	2 (1.39%)	6 (4.17%)	1	0	Cardiovascular
Heart failure	1 (0.69%)	17 (11.81%)	**0.013**	0	Cardiovascular
Extracardiac arteriopathy	0 (0%)	11 (7.64%)	**0.017**	0	Cardiovascular
Pulmonary hypertension	0 (0%)	1 (0.69%)	1	0	Cardiovascular
Ulcerative colitis	0 (0%)	1 (0.69%)	1	0	Digestive
Liver disease	0 (0%)	2 (1.39%)	1	0	Digestive
Diabetes	4 (2.78%)	43 (29.86%)	**<0.001**	0	Metabolic and endocrine
Obesity (BMI >32)	4 (2.78%)	34 (23.61%)	**0.001**	0	Metabolic and endocrine
Arthritis	0 (0%)	4 (2.78%)	0.306	0	Musculoskeletal
Osteoporosis	0 (0%)	1 (0.69%)	1	0	Musculoskeletal
Neurological disease	0 (0%)	1 (0.69%)	1	0	Neurological
Chronic obstructive pulmonary disease	1 (0.69%)	21 (14.58%)	**0.002**	0	Respiratory
Asthma	0 (0%)	5 (3.47%)	0.177	0	Respiratory
Renal disease	0 (0%)	8 (5.56%)	0.055	0	Urogenital
Anaemia	2 (1.39%)	28 (19.44%)	**0.001**	0	Haematological

Table 2 Patients' characteristics *Tests between the groups were conducted by exact test for categorical variables and t-test or non-parametric Wilcox test for continuous variables. Data is presented as n (%) for categorical variables and mean (standard deviation) or median (interquartile range) for continuous variables.

	All patients n=144	Multimorbidity (two or more comorbidities)		Correlations			
		No (n=46)	Yes (n=98)	*p*-value	Estimate	*p*-value	Missing data
Demographics	Age (years)	67.5 (61.25 - 75.5)	70 (63.25 - 73.75)	0.733	-0.007	0.930	0
	Sex - male	40 (27.78%)	82 (56.94%)	0.804			0
	BMI	28 (25.25 - 29)	29 (25 - 32.75)	**0.042**	0.288	**<0.001**	0
	Ethnic - White	39 (27.08%)	91 (63.19%)	0.254			0
	Smoking						
	never smoker	16 (11.11%)	36 (25%)				
	ex-smoker	25 (17.36%)	50 (34.72%)	0.967			0
	current smoker	5 (3.47%)	12 (8.33%)				
Medication	Statin	39 (27.08%)	83 (57.64%)	1			0
	Antidiabetic medication						
	Alogliptin	0 (0%)	1 (0.69%)				
	Gliclazide	0 (0%)	5 (3.47%)				
	Insulin	0 (0%)	6 (4.17%)	**0.011**			0
	Linagliptin	0 (0%)	1 (0.69%)				
	Metformin	2 (1.39%)	17 (11.81%)				
	Anti-platelet (5 days pre surgery)	34 (23.61%)	74 (51.39%)	0.839			0
	ACE inhibitor	16 (11.11%)	44 (30.56%)	0.281			0
Clinical characteristics	*Surgery type*						
	CABG	38 (26.39%)	86 (59.72%)	0.441			0
	CABG & Valve	7 (4.86%)	11 (7.64%)	0.441			0
	CABG & Valve & Other	0 (0%)	1 (0.69%)	0.441			0
	Valve & Other	1 (0.69%)	0 (0%)	0.441			0
	NYHA						
	class I	18 (12.5%)	21 (14.58%)				
	class II	27 (18.75%)	60 (41.67%)	**0.006**			0
	class III, IV	1 (0.69%)	17 (11.81%)				
	CCS						
	asymptomatic	10 (6.94%)	11 (7.64%)				
	class I	23 (15.97%)	16 (11.11%)				
	class II	11 (7.64%)	46 (31.94%)	**<0.001**			0
	class III	2 (1.39%)	14 (9.72%)				
	class IV	0 (0%)	11 (7.64%)				
	LVEF						
	Fair (30-49%)	5 (3.47%)	20 (13.89%)	0.237			0
	Good (>49%)	41 (28.47%)	78 (54.17%)				
	Left main stem diseased	10 (6.94%)	31 (21.53%)	0.242			0
	Extent of coronary disease						
	Normal	3 (2.08%)	3 (2.08%)				
	1VD	4 (2.78%)	2 (1.39%)	0.186			0
	2VD	11 (7.64%)	25 (17.36%)				
	3VD	28 (19.44%)	68 (47.22%)				
Preoperative characteristics	PaO2/FiO2 ratio baseline	495.26 (409.52 - 690.48)	457.18 (409.52 - 533.33)	0.572	-0.055	0.513	0
	MABP baseline (mm Hg)	96.75 (87.25 - 104)	95.5 (88 - 102.75)	0.771	-0.012	0.884	0
	Serum creatinine baseline (umol/L)	85 (76.25 - 95.75)	83.5 (75.25 - 94)	0.656	0.047	0.575	0
	Bilirubin baseline (umol/L)	10 (8 - 13)	10.5 (8 - 13)	0.889	-0.041	0.626	3
	Platelets baseline (x109/L)	212.5 (171.25 - 236.5)	235 (186 - 269)	0.069	0.145	0.084	0
	Haemoglobin baseline (g/L)	142.5 (137.25 - 149)	140 (127 - 151)	0.107	-0.204	**0.014**	0
	Haematocrit baseline (%)	0.42 (0.04)	0.41 (0.05)	0.169	-0.145	0.083	0
	Red blood cells baseline	4.72 (4.43 - 5.01)	4.58 (4.23 - 4.91)	0.093	-0.138	0.100	0
	White blood cells baseline	6.8 (5.8 - 8.68)	7.9 (6.73 - 9)	**0.021**	0.233	**0.005**	0
	Lymphocytes baseline	1.71 (1.45 - 2.26)	1.92 (1.47 - 2.36)	0.229	0.187	0.025	0
	Monocytes baseline	0.5 (0.38 - 0.6)	0.5 (0.4 - 0.61)	0.415	0.113	0.179	0
	Neutrophils baseline	4.26 (3.34 - 5.5)	5.01 (3.95 - 5.9)	**0.024**	0.154	0.066	0
	Eosinophils baseline	0.17 (0.11 - 0.29)	0.22 (0.13 - 0.31)	0.195	0.181	**0.030**	0
	Basophils baseline	0.04 (0.03 - 0.05)	0.04 (0.03 - 0.06)	0.089	0.189	**0.023**	0
Postoperative characteristics	PaO2/FiO2 ratio (CICU)	266.27 (221.74 - 317.97)	256.27 (193.7 - 351.78)	0.586	-0.168	**0.044**	0
	MABP (CICU) (mm Hg)	75 (64.25 - 84.75)	72 (65 - 81)	0.581	-0.041	0.626	0
	Serum creatinine (CICU) (umol/L)	78 (66.25 - 85)	78.5 (68 - 91.5)	0.433	-0.040	0.635	0
	Bilirubin (CICU) (umol/L)	12 (9.25 - 15.75)	12 (10 - 16)	0.929	0.139	0.097	2
	Platelets (CICU) (x109/L)	162.5 (134 - 214)	179.5 (154 - 225.25)	0.079	0.199	**0.018**	2
	Haemoglobin (CICU) (g/L)	110.5 (105 - 122.75)	109 (101 - 120)	0.124	-0.039	0.641	0
	Haematocrit (CICU) (%)	0.33 (0.04)	0.33 (0.05)	0.434	-0.037	0.657	0
	Red blood cells (CICU)	3.72 (0.5)	3.62 (0.5)	0.255	0.041	0.624	0
	White blood cells (CICU)	13.35 (10.75 - 18.75)	14.85 (11.2 - 19.23)	0.442	0.098	0.244	0
	Lymphocytes (CICU)	1.21 (1.03 - 1.93)	1.43 (1.12 - 1.91)	0.336	0.131	0.119	0
	Monocytes (CICU)	0.6 (0.34 - 0.79)	0.66 (0.4 - 0.9)	0.182	0.126	0.133	0
	Neutrophils (CICU)	10.7 (8.17 - 14.41)	12.16 (8.82 - 15.81)	0.17	0.098	0.242	0
	Eosinophils (CICU)	0.15 (0.08 - 0.21)	0.12 (0.08 - 0.19)	0.481	-0.032	0.706	1
	Basophils (CICU)	0.03 (0.02 - 0.04)	0.03 (0.02 - 0.05)	0.069	0.180	**0.031**	1
	Lactate (CICU) (mmol/L)	1.55 (1.1 - 2.1)	1.9 (1.4 - 2.5)	**0.013**	0.191	**0.023**	1
	MODS (CICU)	2 (1 - 3.5)	2 (1 - 3)	0.71	0.096	0.268	8
	Inotropic score 24h	0 (0 - 2)	0 (0 - 3)	0.418	0.002	0.979	8
	Vasoactive score 24h	7 (2.5 - 73.5)	7 (3 - 17)	0.841	0.020	0.822	8
	PaO2/FiO2 ratio 24hr	358.33 (300 - 409.52)	347.62 (263.07 - 456.93)	0.538	-0.139	0.098	1
	MABP 24hr (mm Hg)	85.3 (80 - 95.5)	83 (75 - 95)	0.233	-0.049	0.561	1
	PaO2/FiO2 ratio 48h	358.33 (301.79 - 409.52)	356.94 (273.31 - 410.85)	0.96	-0.148	0.078	2
	serum creatinine 48h (umol/L)	77 (70 - 92.25)	74 (65 - 93)	0.439	0.138	0.110	3
	post-op RBC transfusion	14 (9.72%)	37 (25.69%)	0.457			0
	nonRBC transfusion >48h postop	8 (5.63%)	9 (6.34%)	0.162			2
	nonRBC transfusion <=48h	5 (3.68%)	12 (8.82%)	1			8
	PaO2/FiO2 ratio 48hr <=300	12 (8.33%)	30 (20.83%)	0.695			0
	AKI - kdigo criteria	1 (0.69%)	11 (7.64%)	0.104			0

Figure 1

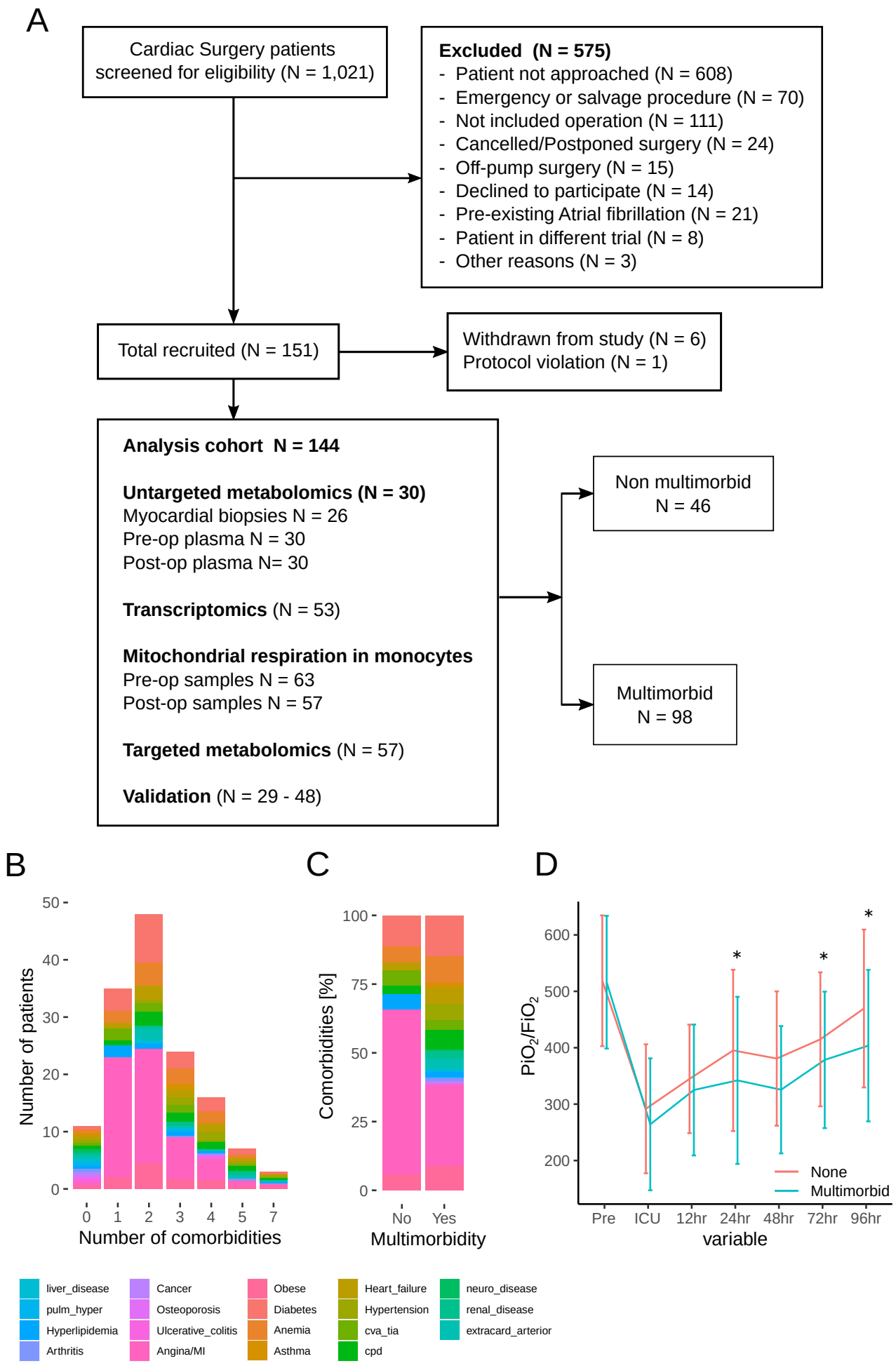

Figure 2

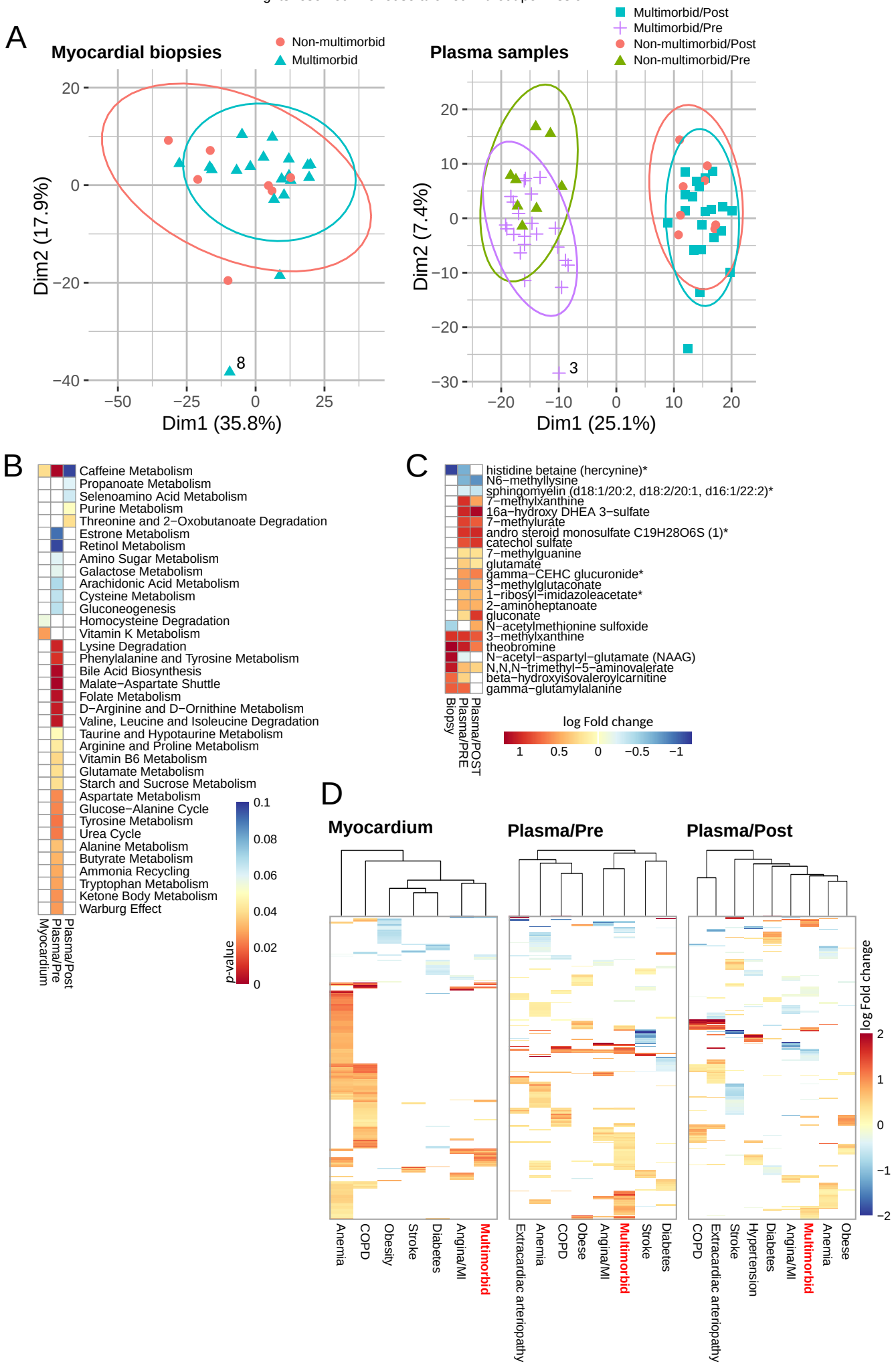

Figure 3

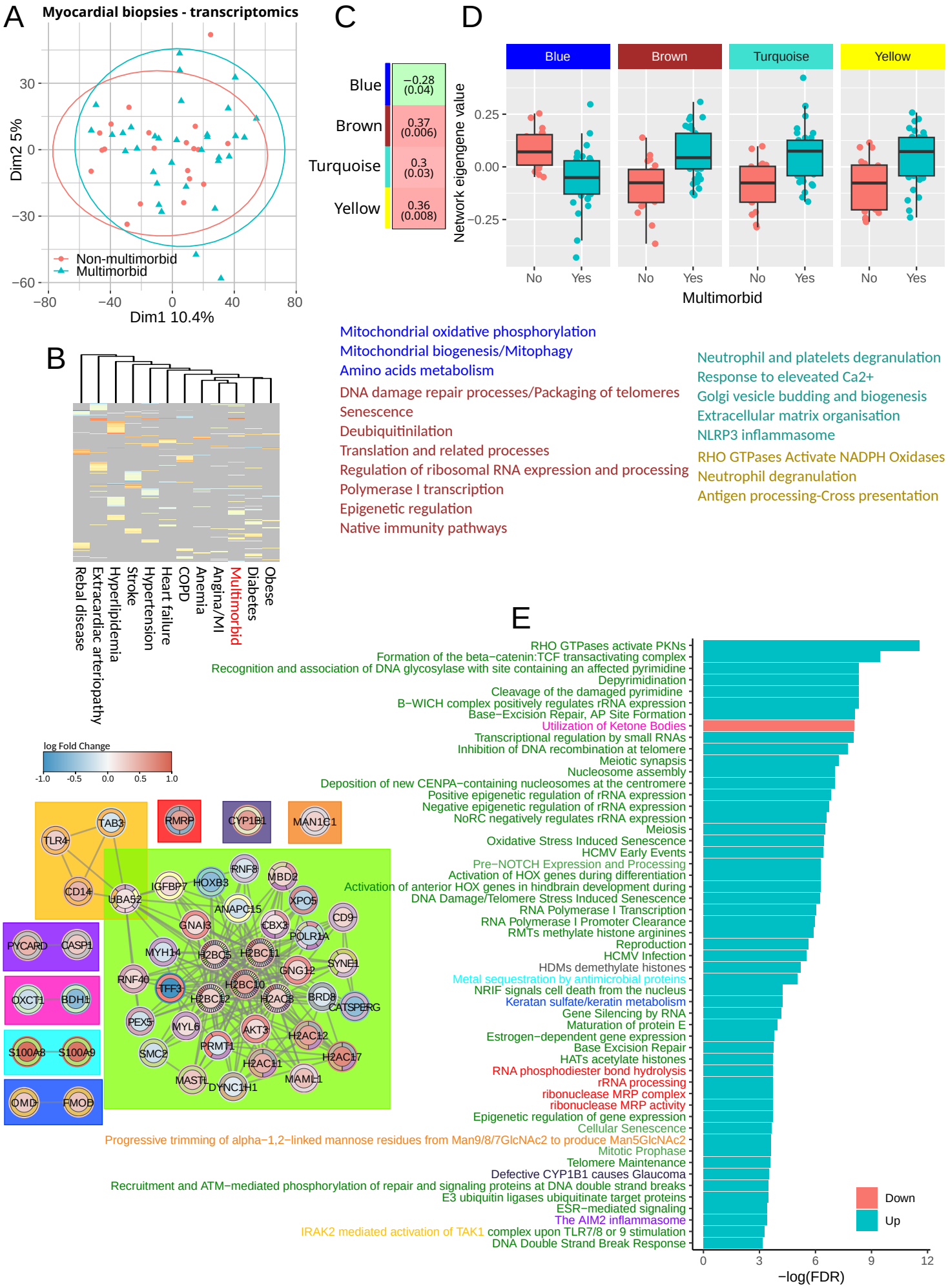

Figure 4

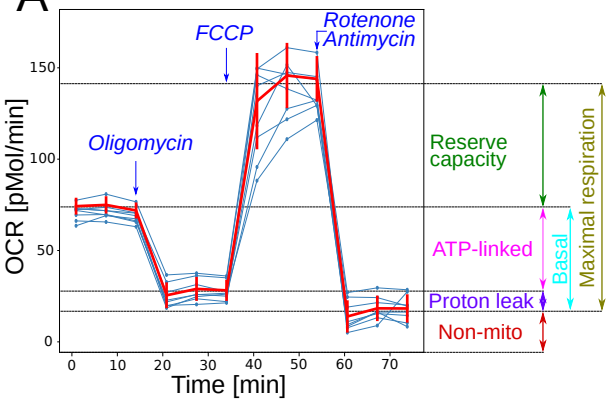

	Variable	N	Multimorbid (SD)	Non-multimorbid (SD)	p-value
Pre	ATP_linked	63	37.053 (12.943)	38.767 (12.544)	0.651
	Baseline	63	63.211 (18.355)	63.616 (20.892)	0.947
	Maximal	63	4.335 (0.472)	4.415 (0.469)	0.571
	Proton leak	63	8.298 (3.586)	7.624 (2.993)	0.475
	RCR_{basal}	**63**	**5.114 (2.204)**	**6.669 (2.454)**	**0.039**
	RCR_{max}	**63**	**7.464 (4.858)**	**10.719 (5.896)**	**0.040**
	Spare	63	24.425 (30.517)	29.941 (24.137)	0.168
	$Maximal_{Pyr}$-$Maximal_{Glucose}$	62	56.992 (18.662)	55.697 (23.914)	0.850
Post	ATP-linked	57	41.836 (16.044)	38.722 (12.125)	0.449
	Baseline	57	72.564 (20.769)	65.511 (22.945)	0.319
	Maximal	57	98.355 (37.449)	100.27 (49.837)	0.896
	Proton leak	57	7.792 (4.555)	8.082 (4.515)	0.837
	RCR_{basal}	57	6.71 (3.993)	6.552 (4.412)	0.711
	RCR_{max}	57	9.819 (7.132)	11.02 (8.427)	0.553
	Spare	57	30.368 (28.38)	36.664 (35.046)	0.582
	$Maximal_{Pyr}$-$Maximal_{Glucose}$	54	64.077 (25.289)	60.773 (26.855)	0.708

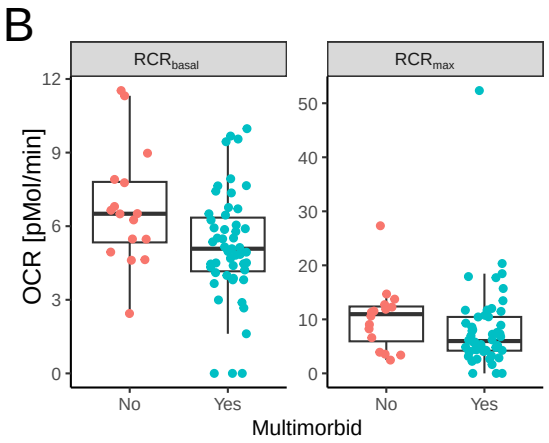

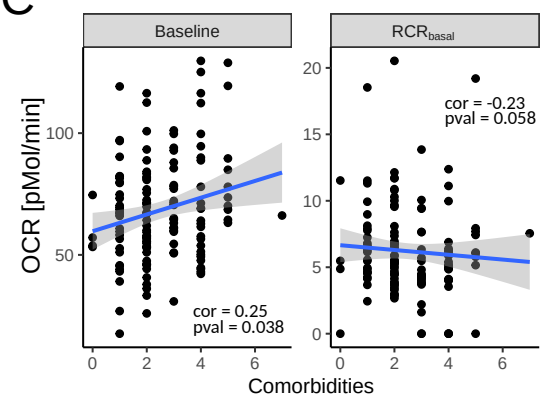

D

	Variable	N	Multimorbid (SD)	Non-multimorbid (SD)	p-value
Pre	Baseline	67	1.801 (0.486)	2.004 (0.618)	0.257
	GRC	67	2.523 (2.222)	2.479 (1.394)	0.391
	Oligomycin	67	2.081 (0.552)	2.276 (0.574)	0.257
	Rotenone/Antimycin	67	1.87 (0.813)	2.134 (0.827)	0.285
Post	Baseline	66	2.269 (0.635)	2.42 (0.717)	0.449
	GRC	66	2.17 (2.318)	2.859 (2.571)	0.243
	Oligomycin	66	2.421 (0.648)	2.559 (0.822)	0.538
	Rotenone/Antimycin	66	13.519 (11.663)	17.633 (15.23)	0.298

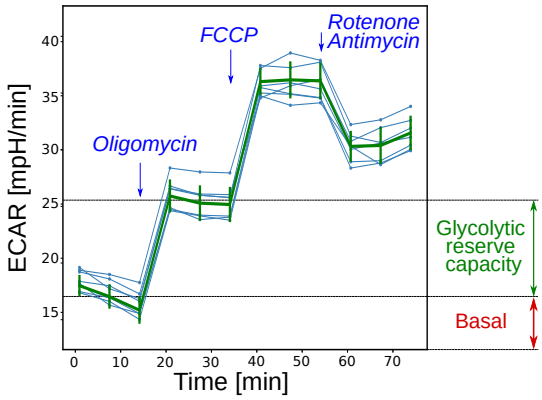

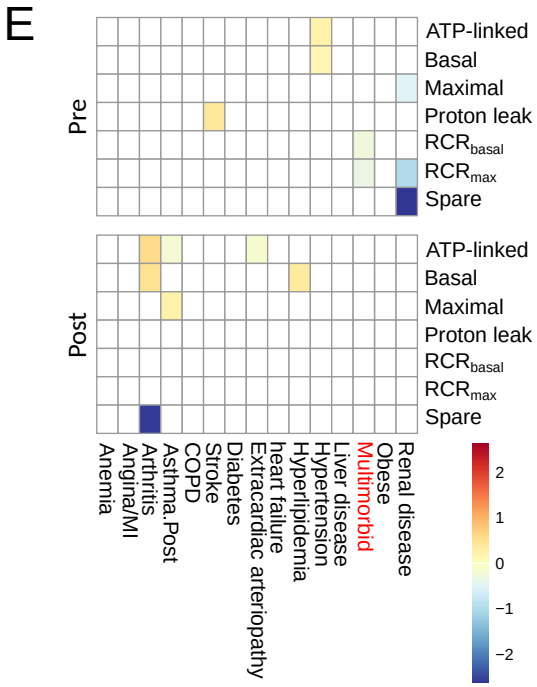

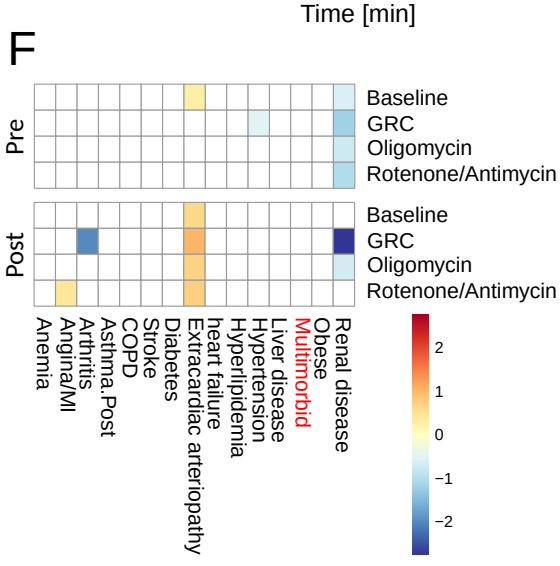

Figure 5

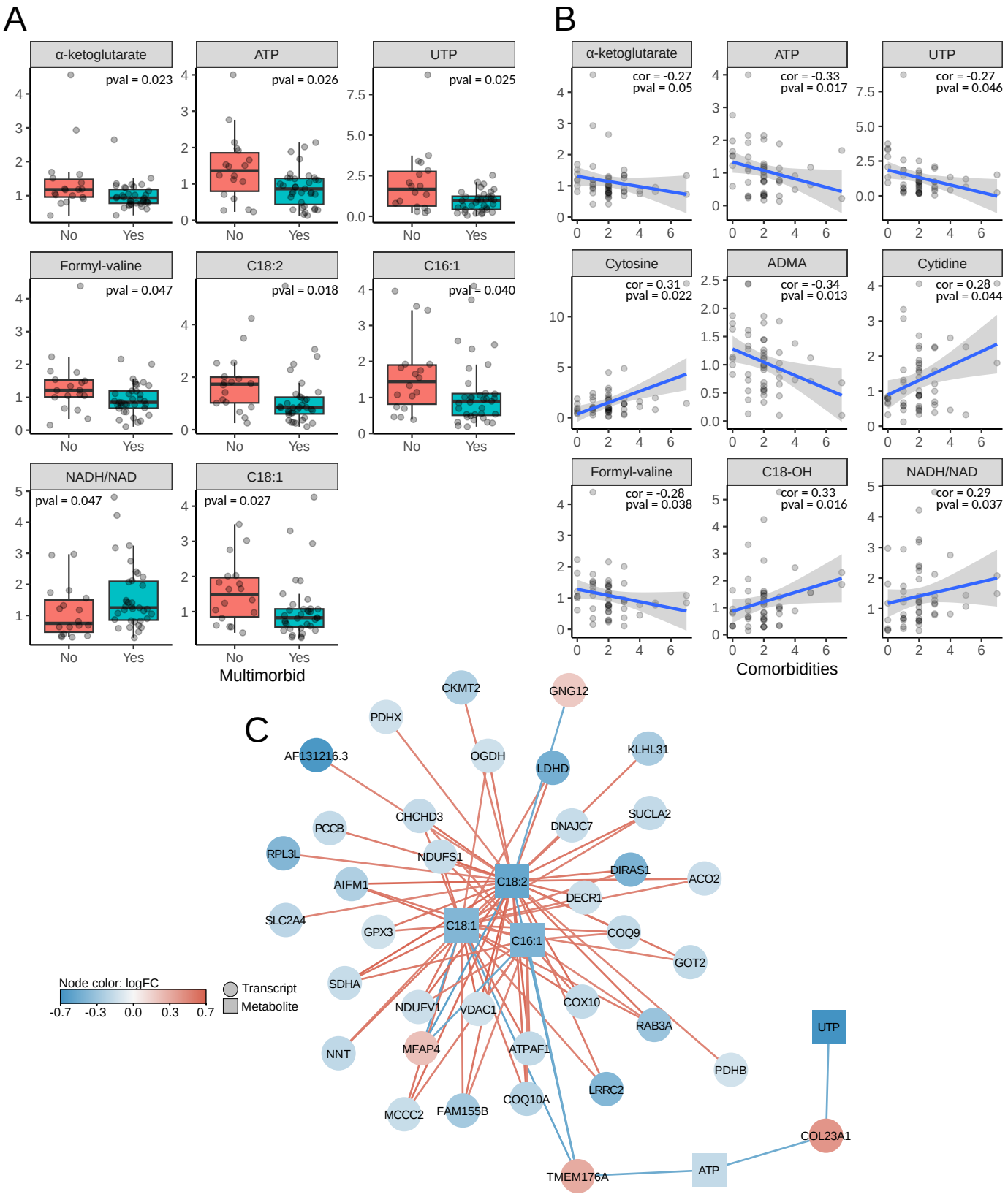

Figure 6

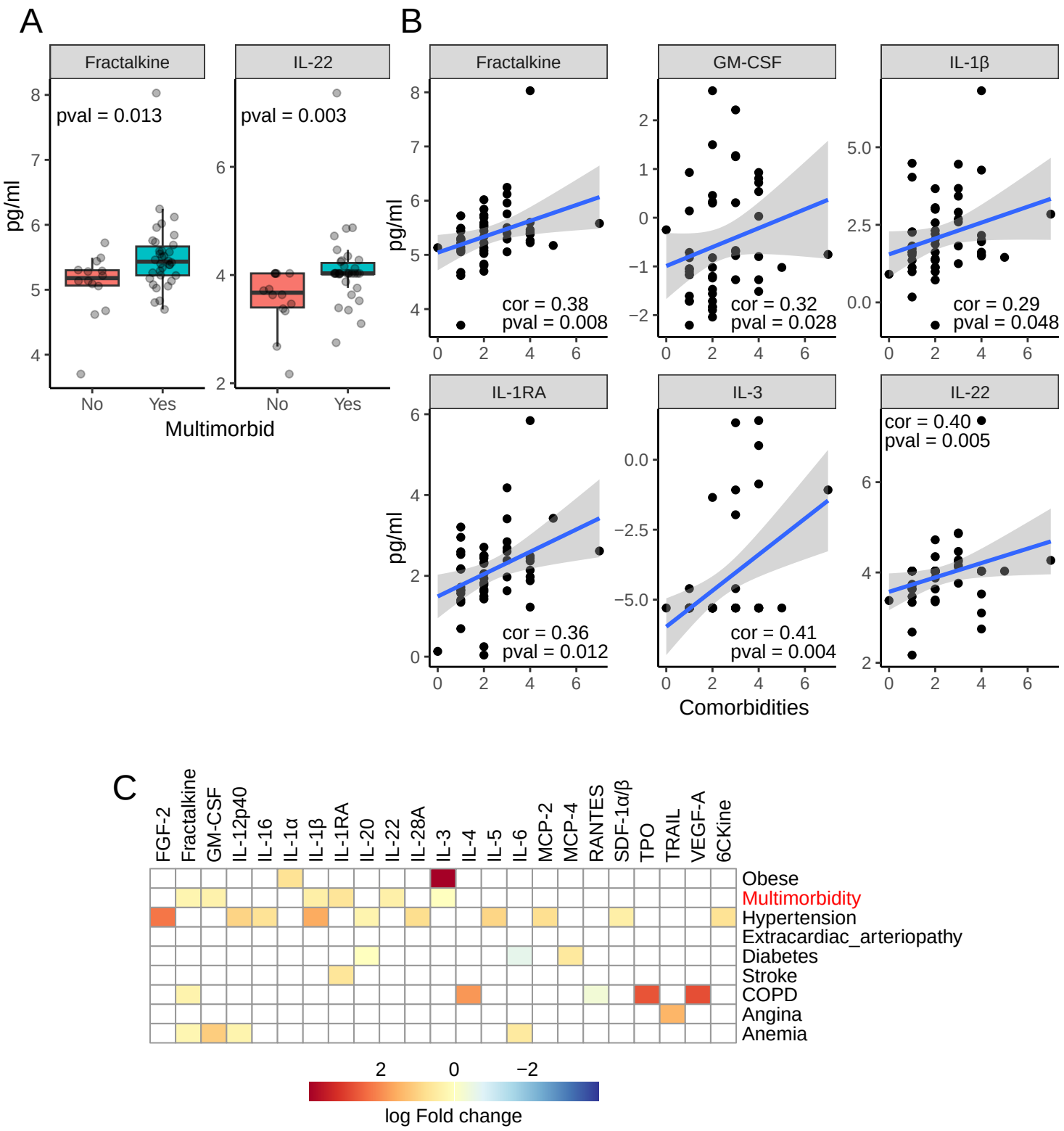

Figure 7